Multiple activities of the MatP protein are involved in post-replicative pairing of sister chromosomes in *Escherichia coli*

Estelle Crozat[1,2,*], Catherine Tardin[3], Maya Salhi[1], Philippe Rousseau[1], Armand Lablaine[1], Tommaso Bertoni[2], David Holcman[4], Bianca Sclavi[5], Pietro Cicuta[2], and François Cornet[1]

[1] Centre de Biologie Intégrative de Toulouse (CBI Toulouse), Laboratoire de Microbiologie et de Génétique Moléculaires (LMGM), Université de Toulouse, CNRS, UPS, France.

[2] Cavendish Laboratory, University of Cambridge, Cambridge CB3 0HE, United Kingdom

[3] Institut de Pharmacologie et de Biologie Structurale (IPBS), Université de Toulouse, CNRS, UPS, France.

[4] Ecole Normale Supérieure, Applied Math and Computational Biology, IBENS, 46 rue d'Ulm, 75005, Paris, France

[5] Laboratory of Biology and Applied Pharmacology (UMR 8113 CNRS), Ecole Normale Supérieure, Paris-Saclay, France

*Corresponding author

Abstract

Regions of the chromosome where replication terminates host specific activities in all organisms. In *Escherichia coli*, this region, named *ter*, is also the last segregated before cell division. Delayed segregation is controlled by the MatP protein, binding specific *matS* sites along *ter*. We investigated the fate of the *E. coli ter* region and the role of MatP by combining a detailed *in vivo* analysis of the mobility of a *ter* locus at short time scales with *in vitro* biochemical approaches. We found that *ter* dynamics differs only slightly from that of a control locus located close to the replication origin, except when sister *ter* loci are paired following their replication. MatP thus mainly acts in maintaining sister *ter* paired, but only plays a faint role in absence of pairing. This effect depends on MatP, its 20 C-terminal residues and ZapB to different levels, implying a role for all known MatP activities. We characterised MatP/DNA complexes and conclude that while MatP binds DNA as a tetramer, it barely forms specific DNA loops by bridging *matS* sites in a DNA rich environment. We propose that tetramerisation of MatP links *matS* sites with ZapB and/or with non-specific DNA to promote optimal pairing of sister *ter* regions until cell division.

The compaction and organization of bacterial nucleoids contribute to an efficient maintenance of the genetic material, integrated with robust yet adaptive expression of genetic programs, in ways that are only partially understood. Nucleoid structuration is due to a variety of processes including DNA supercoiling, proteins and complexes working on the DNA (e.g., RNA polymerases), nucleoid-associated proteins (NAPs) and condensins (SMCs) [1]. These act together to shape the chromosomes in a dynamic structure while keeping DNA accessible to polymerases and repair proteins. Replication and segregation re-organize nucleoids on a large scale [2,3]. Whilst some details of the choreographies depend on the bacterial species, common to all of them is the bidirectional replication of the chromosome, starting at a unique origin and finishing in the opposite terminus region, which is also the last to be segregated before the cell divides.

In bacterial chromosomes, macrodomains are large regions with preferential genetic recombination and specific cellular positioning. Most reported macrodomains contain either the origin or terminus of replication [4–8]. In *Escherichia coli* (*E. coli*), a very distinctive macrodomain (the Ter macrodomain, or *ter*) contains the terminus region and spreads along 765kb, containing 23 *matS* sites that are bound by MatP (Fig. 1A) [9]. MatP is known to play a key role in positioning the chromosome and setting the segregation pattern for *ter*: It keeps the sister *ter* regions together, close to the cell division complex (the divisome; i.e., in the mid-cell area), allowing their processing by the divisome-associated FtsK DNA-translocase [10]. Since FtsK activity is oriented by KOPS DNA motifs, the resulting segregation pattern is precisely oriented and ends at the *dif* site, where final unlinking of sister chromosomes occurs [10,11].

How MatP achieves its functions is currently unclear. MatP forms dimers in absence of DNA, and tetramers upon binding to *matS*-containing DNA [12]. This was proposed to pair distant *matS* sites, forming large chromosome loops organising *ter*. Such interactions were however not detected in contact maps of the chromosome [13]. MatP was also shown to interact with the divisome-associated ZapB protein [14] and the condensin MukB [15]. Neither interaction has been deeply characterized so far. A truncated variant of MatP (deletion of the 20 last residues), MatPΔ20, was reported unable to form tetramers [12] nor to interact with ZapB [14], yet retaining interaction with MukB [15]. MukB was recently reported to promote long-range interaction between chromosome loci, except into *ter* where it has no effect [13]. This exception of *ter* seems to be dependent of MatP since it is not observed in a *ΔmatP* strain. In addition, MatP, as well as MatPΔ20, promotes short-range interactions inside *ter* [13]. On the other hand, a MukB variant, defective in ATP hydrolysis, binds *matS* sites in a MatP-dependent manner, which is barely detected in a wild type strain [15]. Taken together, these results suggest that MatP excludes MukB from *ter*. Since MukB interacts with TopoIV, its exclusion by MatP has been proposed to delay decatenation of sister *ter*, thus coupling their segregation with cell division. Interaction of MatP with ZapB has been proposed to be involved in a positive control of divisome assembly around *ter*, an effect referred to as the Ter-linkage [16,17]. Mutation of *zapB* alters the

mid-cell positioning of MatP-bond sister *ter* and shortens the co-localization times of *ter* loci [14]. The dynamics of *ter* loci is affected consistently in a *matP*Δ*20* strain [12].

Beside the subcellular positioning and segregation time of chromosome loci, their movements have been recorded at different time scales, revealing important differences between chromosome regions. At long time-interval scales (i.e., looking at displacements above one minute), loci tracking captures their segregation dynamics as well as rapid super-diffusive movements unrelated to segregation per se [18–23]. Loci of *ter* localize accurately when in the mid-cell zone [18]. Their separation occurs at mid-cell at a time in the cell cycle when at least early divisome components have formed a complex at mid-cell. At short time-intervals, tagged chromosome loci sub-diffuse, i.e., they explore space slower than they would due to Brownian motion [20,24–26]. This reflects constraints imposed by their environment and is directly correlated with their capacity to interact with distant loci [9,13,26]. Using single tracks recorded at short time scales and extraction of biophysical properties, a previous study showed that the mobility of loci varied depending on chromosomal localization [26], with the *ter* loci less mobile (more constrained) when located at mid-cell.

In this report, we investigate the role of MatP in constraining the mobility of a *ter* locus. We first show that mobility depends on the system used to tag loci, on the intensity of fluorescent foci and their cellular positioning. Surprisingly, low-fluorescent foci of the *ter* locus were as mobile as those of an *oriC*-proximal locus, showing that the higher constraint of the *ter* locus is not an intrinsic property of this chromosome region but depends on context. We further show that highly intense and poorly mobile foci form most often at the *ter* locus and depend on the presence of MatP, suggesting they contain pairs of unsegregated sister loci. This effect depends on MatP, its 20 C-terminal residues and ZapB to different levels, implying a role for all known MatP activities. We characterised MatP/DNA complexes and conclude that while MatP binds DNA as a tetramer, it barely forms specific DNA loops by bridging *matS* sites, in a DNA rich environment, so this tetramerisation serves some other purpose.

Results

Monitoring chromosome loci mobility *in vivo*

To monitor the mobility of chromosome loci, we used strains carrying a *parS* site inserted in the *ori* or *ter* regions of the chromosome and producing cognate ParB proteins fluorescent derivatives [27] (Fig. 1a). We recorded the position of foci every 0.5s during 20s (Fig. 1b). We then extracted the mean squared displacements (MSD) from these trajectories. An example of 30 MSD for the Ter4 locus is shown in Fig. 1c.

We first used the P1 *parS* site and ParB protein to tag loci in the *ori* and *ter* regions. Using this system, we reproduced results previously reported for the Ori2 and Ter3 loci [26] (Fig. 1e). However, this P1-derived system has been reported to induce increased post-replicative cohesion of

tagged loci [10]. We thus also used another set of strains, with loci tagged by insertion of the pMT1 *parS* site and producing a ParB-pMT1 fluorescent derivative [27]. Comparing the two tagging systems revealed very important differences: (i) The number of cells with a single focus increased and those with two foci decreased when using the P1-derived system compared to the pMT1-derived system (Fig. 1d); (ii) The MSDs obtained with the pMT1 system were higher than with the P1 system (Fig. 1e); (iii) The difference in MSDs between the *ori* and *ter* loci was largely reduced when using the pMT1-derived system (Fig. 1e); (iv) For a same intensity (1000 AU for instance), a remarkable drop of mobility was observed only for Ter loci labelled with ParS-P1 [26]. The P1-derived system thus not only delays *ter* segregation, but creates aggregates of proteins that resulted in brighter foci (Fig. S1) with very low mobility, biasing the results obtained with this system. We chose to proceed exclusively with the pMT1-derived system in this work.

The low mobility of a *ter*-proximal locus depends on foci intensity

We next analyzed the fate of foci formed at the Ori2 and Ter4 loci using the pMT1-derived system. Foci populations were binned into categories depending on their number per cell (either one or two in our growth conditions) and their localization in the cell for which we defined two categories: (M) midcell (0-0.16 cell length from the cell center) and (R), rest of the cell (0.17-0.5). Foci of the Ori2 locus were preferentially localized at the quarter positions in cells with two foci and between the mid-cell and quarter positions in cells with a single focus (Fig. S2). This was consistent with previously reported positioning of the *ori* region before and after its segregation [28–30]. Also consistent with previous reports, foci of the Ter4 locus were preferentially located in the mid-cell area (Fig. S2), unsegregated (single) foci being closer from mid-cell than segregated (double) ones.

The intensity of foci varied between the *ori*- and *ter*-proximal loci. Foci formed at the Ori2 locus followed a sharp distribution centered around 500 AU (Fig. 2a). In contrast, foci formed at the Ter4 locus followed a wider distribution with a higher proportion of highly intense foci. For moderately intense foci, we observed a monotonous decrease of foci mobility when their intensity increased (Fig. 1f). Strikingly, Ori2 and Ter4-borne loci had the same MSDs at corresponding intensities. The low mobility of *ter* loci repeatedly reported [20,26,31] is thus not an intrinsic property of *ter* loci but depends on the intensity of foci. This was however only true for moderately intense foci, below 1000 AU of fluorescence (Fig. 1f). At higher intensities, foci mobility no longer varies in a monotonous way with increasing intensity and was clearly different between the Ori2 and Ter4 loci (Fig. 1f). From this observation, we defined two categories of foci: foci of low intensity, hereafter called FL, below 1000 AU, and foci of high intensity, hereafter called FH, above 1000 AU. FH were rare at the Ori2 locus (2%) but rather frequent at Ter4 (30%) (Fig. 2b). Single foci of Ter4 were located closest to mid-cell than double foci (Fig. 2c). Double FH were rare and tended to position like double FL.

We performed a calibration by extracting the number of GFP molecules in a focus from the increase of variance in intensity along time. This gave an estimated mean of 33 GFP molecules per

focus for Ter4, FL foci, whereas the mean for Ter4, FH foci was 70 GFP (Fig. S3 and Supp. mat.). The mean obtained for Ori2 foci was 33 GFP molecules per focus.

Foci of high and low intensities show different dynamics

We analyzed the trajectory of foci using four parameters providing independent information about the nature of locus movement, described in materials and methods and following the work by Amitai and coworkers [32]: (i) The anomalous exponent (α) is computed from the auto-correlation function behavior for small increments. It indicates the nature of the locus motion. α=1 describes normal diffusion, while α<1 is sub-diffusive (constrained) and α>1 is super-diffusive (directed) movement (Dion and Gasser, 2013). (ii) The length of confinement (L_c) is defined as the standard deviation (SD) of the locus position with respect to its mean averaged over time. This provides estimation for the apparent radius of the volume explored by a finite trajectory. (iii) The diffusion coefficient (D_c) reflects the second order statistical properties of a trajectory. This diffusion coefficient accounts for local crowding that may vary along the trajectory. (iv) The effective spring coefficient (K_c) represents an external force acting on a chromosomal locus. It is modelled as a spring force applied on a single monomer belonging to a polymer. This force affects the entire polymer motion and can be recovered from the first order moment statistics of single locus trajectories.

Considering only foci of low intensity (FL) (Fig. 2d), the value of each parameter was poorly dependent of the position of the focus in the cell, suggesting that loci properties do not change significantly during the cell cycle. Ori2 foci had a low value of α (0.16), whereas Ter4 showed a slightly higher α (0.2). According to the RCL model [32–34], this suggests that the DNA is locally condensed for both loci, but slightly more in *ori* than in *ter.* The length of confinement for both foci was small (0.084 and 0.081µm for Ori2 and Ter4, respectively), revealing that loci are confined in small regions, the size of which does not change much with chromosomal or cellular location. The effective diffusion coefficient was higher for Ori2 than Ter4 (3.5 $x10^3$ and 2.9 $x10^3 \mu m^2/s$, respectively), showing that despite a higher condensation, Ori2 is freer to diffuse than Ter4. Finally, the spring coefficient reveals high forces tethering both Ori2 and Ter4 (331 and $319 k_B T/\mu m^2$), compared to the values obtained for the *mat* locus in budding yeast ($90 k_B T/\mu m^2$, [32]). In cells harboring two foci, FL showed the same behavior as in cells with a single FL (Fig. S4a).

Highly intense foci of the Ter4 locus (Ter4 FH) behaved differently than FL (Fig. 2d). Ter4 FH α was close to the FL value (0.22 for FH and 0.2 for FL, $p=10^{-5}$) and remained the same for both cell positions (p=0.5), suggesting a monotonous condensation of the *ter* region. However, L_c was lower than for FL ($p=10^{-125}$) and lower at mid-cell than in the rest of the cell ($p=8.10^{-4}$). This suggested that Ter4 FH are more confined than FL and more confined when in the mid-cell than other cell areas. D_c showed the same trends as L_c, showing that Ter4 FH are diffusing less than FL ($p=10^{-200}$) and less when in the mid-cell area ($p=5.10^{-5}$). These changes are consistent with an increase - nearly doubled - in the force applied to Ter4 in FH when in the mid-cell area ($620 k_B T/\mu m^2$ for FH at mid-cell and $331 k_B T/\mu m^2$ for FL, $p=10^{-130}$).

Ter4 FH were thus: more intense than FL; submitted to twice the force compared to FL, particularly when present at mid-cell; more confined and less diffusive than FL and most preferentially located at mid-cell. A straightforward hypothesis is that they mostly contain sister Ter4 loci held together in post-replicative cohesion. This hypothesis is consistent with the extended cohesion period reported for sister *ter* regions [20,28,30], even when the pMT1-derived localization system was used [10]. This also explains the higher percentage of FH for the Ter4 compared to the Ori2 locus. It follows that most FL contain single copies of loci. Assuming this hypothesis, a strong constrain is applied to *ter* loci only when they are in post-replicative cohesion. The rest of the time, their dynamics is much less different from other chromosome regions than previously thought.

MatP is required for FH formation and maintenance at the *ter* locus

We next deleted *matP* from our labelled strains and observed the fate of Ter4 foci. The strongest effect was on FH. Cells with one FH decreased drastically (from 27% to 8%; Fig. 3a) whereas cells with one FL decreased moderately (from 58% to 48%). Consistently, cells with two foci raised and mostly contained FL. This increase in two-foci cells is consistent with previous reports positing that MatP acts to keep sister *ter* regions together after replication [9]. The large decrease in cells with one FH thus confirms that FH contain pairs of unsegregated sister loci. In the Δ(*matP*) strain, the remaining FH were more mobile and less confined than in the wild type strain. They showed increased L_c and D_c values and decreased K_c values (Fig. 3b, $p=10^{-8}$, $p=1.9\ .10^{-12}$, $p=7.6\ .10^{-11}$, respectively). These values were close to the ones obtained for Ori2 FH (Table S2, p=0.75, $p=4.10^{-3}$, p=0.56 for for L_c, D_c and K_c). In addition, no more difference was observed with cell positioning, meaning that FH at mid-cell were not different anymore from the ones located in the rest of the cell (Fig. 3b, p=0.6, p=0.4, p=0.5 for L_c, D_c and K_c). We conclude that MatP is required both for the high number of FH foci at the Ter4 locus and for their specific constrain when located at mid-cell. A slight but significant difference in mobility and confinement between FH and FL in the Δ(*matP*) strain remains (Fig. 3; Table S2, $p=4.10^{-17}$, $p=2.10^{-33}$ and $p=4.10^{-14}$ respectively for L_c, D_c and K_c). This difference might be explained by the higher intensity of FH, which should reduce their mobility [35]. Interestingly, deletion of *matP* had only a slight effect on the α coefficient of Ter4 foci for FH (p=0.02) and none on FL (p=0.06), suggesting MatP only marginally influences the local condensation of *ter* DNA.

Deleting *matP* also had a small but significant effect on Ter4 FL dynamics (Fig. 3c). Ter4 FL were less confined and more mobile in the Δ(*matP*) than in the wild type strain (higher L_c ($p=3.10^{-7}$) and D_c ($p=6.10^{-7}$), lower K_c ($p=7.10^{-10}$)). This appears as a general effect (not specific to the *ter* region) as equivalent variations were observed with the Ori2 locus (Fig. S5b).

At least two different activities of MatP are required for FH formation and maintenance

To get more insight into the roles of MatP, we used two other mutants: a deletion of *zapB*, coding for the divisome-associated protein interacting with MatP [14,36] and an allele of *matP*,

matPΔ20, coding for a version deleted of the last 20 C-terminal residues, reported defective for both interaction with ZapB and tetramerisation [12]. In these two mutants, MatP still binds *matS* sites ([12], and below) and interacts with MukB [15].

Both Δ(*zapB*) and *matPΔ20* mutants showed a phenotype intermediate between the wild type and Δ(*matP*) strains considering the populations of Ter4 foci (Fig. 3a). Cells with two FL rose whereas cells with a single FH decreased. This effect was slightly more pronounced in the Δ(*zapB*) than in the *matPΔ20* strain. This suggests that the interaction with ZapB is the main reason of FH foci formation, but tetramerisation of MatP and a third activity that certainly involves interaction with MukB are probably involved too.

Detailed analysis of Ter4 FH behavior in the two mutant strains was fully consistent with the above conclusion (Fig. 3b, Table S3). FH confinement decreased and mobility increased (higher L_c and D_c, lower K_c) compared to the wild type strain; these effects were more marked in the *matPΔ20* strain, but lower than in the Δ(*matP*) strains. In both mutant strains, FH were more confined and less mobile when located at midcell, as in the wild type strain. This suggests that MatP activities other than tetramerisation and interaction with ZapB are sufficient to determine a specific behavior of FH in the mid-cell area.

In the *matPΔ20* strain, Ter4 FL behaved as in the Δ(*matP*) strain (Fig. 3b, Table S3), *i.e.*, slightly increased L_c and D_c and decrease in K_c compared to the wild type strain, indicating a moderate decrease of confinement and increase in mobility. MatP activities other than tetramerisation and/or interaction with ZapB are thus not required to constrain FL. Surprisingly, the Δ(*zapB*) mutation had a larger effect than either the Δ(*matP*) or the *matPΔ20* mutation on Ter4 FL (Fig. 3c). This was unexpected but may be explained by properties of ZapB independent of its interaction with MatP (see discussion). Whatever the reasons, this precluded conclusions on the relative contribution of MatP tetramerisation and interaction with ZapB on FL behaviour.

MatP bridges DNA molecules *in vitro*

As we assume highly fluorescent foci contain paired loci depending on MatP, we attempted to characterize DNA bridging by MatP. Indeed, MatP tetramers were predicted from structural data and chromatography experiments and have the potential to bridge distant *matS* sites [12]. Consistently, DNA bridges via MatP were observed in atomic force and electron microscopies although with poor specificity for *matS* sites [12]. We first designed an assay based on DNA pull-down (Fig. 4a). Briefly, a biotinylated DNA molecule containing 0, 1 or 2 *matS* sites (DNA_b) was bound to a streptavidin-covered magnetic bead. This bead-DNA (DNA_b) complex was mixed with a shorter free DNA (DNA_f) containing 0 or 2 *matS*. The mix was then incubated with purified MatP protein, washed, pulled down with a magnet and eluted in presence of a low concentration of SDS. The amount of DNA_f recovered after elution represents the capacity of MatP to bridge the two DNA molecules (Fig. 4b). When the two DNAs contained two *matS* sites, 18% of DNA_f were recovered with the lowest concentration of

MatP used (0.1µM), increasing to 63% at the highest concentration of MatP used (2µM). We concluded that MatP is able to bridge independent DNA molecules containing *matS* sites. This interaction was stable enough to persist during the course of our experiment. When repeating the same experiment with DNA molecules that did not contain *matS* sites, DNA_f was readily recovered although with lower efficiency (Fig. 4b, right panel). Adding one *matS* on DNA_b increased the amount of DNA_f recovered to an intermediate level (Fig. S6). Thus, MatP can bridge independent DNA molecules, even devoid of *matS* sites. The presence of *matS* stimulates this activity and/or stabilised the complexes formed.

MatP bridging activity involves non-specific DNA binding

To better describe MatP bridging activity, we used a multiplexed tethered particle motion (TPM) set-up [37]. This set-up allows tracking beads attached at one end of a DNA molecule while the other extremity of the DNA is tethered to a coverslip (Fig. 5a and Methods). The amplitude of motion at equilibrium of the bead (A_{eq}) directly depends on the apparent length of the DNA [38]. We used 2284bp long DNAs containing 0, 1 or 2 *matS* sites separated by 1207bp. An example of A_{eq} recorded over time of a single bead is shown Fig. 5b. These traces were plotted as densities of probability of their A_{eq} and fitted to Gaussian distributions (Fig. 5c). Without protein added we observed a single population centered on 250nm (Fig. 5c, *). Adding purified MatP resulted in the displacement of the whole bead population towards shorter A_{eq}, whatever the DNA used. For one part of the population, this corresponded to an apparent shortening of around 30nm (Fig. 5c, **). This moderate decrease in A_{eq} could not correspond to MatP induced DNA looping between the *matS* sites. Indeed, it does not depend on *matS* sites. In addition, even when the DNA contains two *matS*, the shortening predicted from bridging the two *matS* sites is around 100nm. An equivalent moderate decrease in A_{eq} was previously observed using another site-specific DNA binding protein in the same set-up and was inferred to result from protein binding to a single site [39,40]. Surprisingly, this moderate decrease in A_{eq} was not observed with purified MatPΔ20 (Fig. 5c). We verified that MatPΔ20 binds *matS*-containing DNA as well as full length MatP using electromobility shift assay (EMSA; Fig. S7a). Tagged or untagged versions of MatPΔ20 bound a *matS*-containing DNA with at least an equivalent efficiency as MatP. However, the complex formed appeared different and irrelevant to a simple analysis of their mass. Indeed, the tagged MatPΔ20, formed complexes migrating more quickly than MatP even though it is nearly twice its mass (Fig. 6). Assuming MatPΔ20 binds DNA as a dimer [12], these observations suggest that MatP binds DNA as a tetramer (Fig. 6). This difference may thus account for the difference observed between MatP and MatPΔ20 in our TPM experiments, suggesting the moderate decrease in A_{eq} (Fig. 5c, **) is due to tetrameric MatP binding to a single *matS* site or to non-specific DNA, and inducing a change in DNA conformation.

In addition to the slight decrease in A_{eq} described above, a second population with shorter A_{eq} was obtained upon incubation of the DNA containing two *matS* with MatP (Fig. 5c, ***). Gaussian fitting of this population was centered around 150nm (147nm +/-22), corresponding to the 100nm

shortening predicted for looping between two *matS* sites. Consistent with this hypothesis, this peak was neither observed when using DNA without *matS* nor when using MatPΔ20 (Fig. 5c). However, a second peak was also detected upon incubation of the DNA containing a single *matS* with MatP (Fig. 5c). This peak was centered on 153nm +/-23 and contained about three times fewer events than with the 2 *matS*-containing DNA (percentage of the events of about 13% with 1 *matS* instead of 36% with 2 *matS*). The second peak formed with DNA containing one or two *matS* exhibits very similar centers, as if 1200bp was the most favorable the inter-*matS* distance for looping by MatP. We next repeated TPM experiment using 2 *matS*-containing DNA but in presence of non-specific DNA as a competitor. The moderate decrease in A_{eq} was readily observed as in the absence of competitor DNA (Fig. S8a; **). In contrast, a peak corresponding to larger shortening was not observed, showing that pairing of distant DNA loci by MatP is sensitive to non-specific DNA competition. We then analyzed the kinetics of loop formation when MatP is incubated with DNA containing one or two *matS* (Fig. S8b). It shows that the presence of *matS* enhances the formation of loops by increasing the duration of long-lived looped events.

Taken together, these results show that MatP can pair distant DNA loci in the TPM set-up. This activity depends on the 20 C-terminal residues of MatP, is stimulated by the presence of *matS* but is strongly sensitive to the presence of non-specific DNA.

The above conclusion prompted us to analyze in more detail the MatP/*matS* complexes. Using two different DNA probes of different sizes and labelled with different fluorophores but both carrying a single *matS* site, we performed an EMSA experiment (Fig. S7c). The result shows that MatP/DNA complexes detected in EMSA experiment contain a single DNA molecule. This suggests that in DNA/MatP complexes detected in EMSA experiment, one DNA binding domain is involved in specific interaction with *matS*, while the second is free of DNA. We assume that this DNA-free DNA binding domain could be involved in non-specific interaction with DNA (see discussion).

Discussion

We combined different approaches to investigate the fate of the *ter* region and the role of MatP. This yields several new observations and unexpected conclusions: (i) *ter* loci are not intrinsically less mobile than *ori* loci, even in presence of MatP; (ii) however, a significant proportion of *ter* foci show intense fluorescence, most preferentially at mid-cell and are much less mobile; (iii) the proportion of these foci and their low mobility depend on all described activities of MatP; (iv) MatP binds *matS*-containing DNA as a tetramer but this complex contains only one DNA fragment; (v) bridging *matS*-containing DNA can be observed *in vitro* but is efficiently competed by non-specific DNA. From these observations, we conclude that MatP constrains *ter* mobility only at a specific stage of the cell cycle when replication has terminated and sister chromosomes are paired by their *ter* regions (i.e., in the D period of the cell cycle). MatP does so via at least two activities, only one of which depends on its C-terminal domain. This C-terminal domain is required for tetramerisation and wild type MatP binds *matS*-containing DNA as a tetramer. However, our data indicate that pairing two *matS*-containing DNA by a MatP tetramer is a weak activity, readily challenged by non-specific DNA, that may be irrelevant *in vivo*.

Loci of the *ter* region were repeatedly reported less mobile than other chromosome regions [9,12,14,20]. However, these comparisons did not consider the context of foci, particularly their intensity. Tracking foci over short time-interval, focusing on local DNA constraints, revealed that mobility depends on foci intensity and on their sub-cellular positioning [26]. Our data extend this observation and further show that the localization system used plays an important role. Indeed, using the less invasive pMT1-derived system, significant differences in mobility between an *ori*-proximal and a *ter* proximal locus are observed only for the most intense foci (FH), which explains why these differences were described in experiments where only highly intense foci were detected due to limitations of the microscope setup. Indeed, less intense foci (FL) of the *ter* and *ori* loci show no difference in mobility and the same decrease in mobility when intensity increases (Fig. 1). More detailed analyses of the trajectories of these foci revealed slight but significant differences between *ori* and *ter* loci, of which a decreased α coefficient, suggesting the *ori* region is more condensed than the *ter* region. This is consistent with recently reported images of the *E. coli* nucleoid as a donut in cells rendered round, showing a *ter* region less condensed than the rest of the chromosome [41]. However, despite the *ori* region being more condensed, the *ori* locus appears freer to diffuse than the *ter* locus, as shown by its higher diffusion coefficient. This difference is only partly suppressed by mutation of *matP* and better suppressed by mutation of *zapB* (comparing Fig. 2 and 3). Since ZapB self-assemble into large structures and clusters around *ter* (in a MatP-dependent manner) and the divisome (in a MatP-independent manner) [36], we suspect these cluster limit the diffusion of *ter* loci both in presence and absence of MatP.

Highly fluorescent foci (FH) of the *ter* locus show very distinctive properties. They are less mobile than expected from the global decrease in MSD observed when intensity increases and clearly less mobile than foci of the *ori* locus of same intensity (Fig.1). They are most preferentially

localized at mid-cell and depend on MatP and ZapB (Fig. 2 and 3). They are almost always single foci and in mutant strains, their decrease specifically correlates with increase in two-foci cells (Fig. 3). From these observations, we conclude that most FH contain pairs of sister loci. A rough estimation of cell cycle periods duration agrees with this view. In our strain and growth conditions (MG1655 derivatives grown at 30°C in M9 broth with glucose and casamino acids), about two third of the cells have completed replication [42]. Assuming the *ter* locus segregate at the onset of cell constriction [10] and that about 25% of the cells are constricting in a growing population, the 27% FH we observed can be restricted to cells having completed replication and not initiated constriction. Detailed analysis shows that the α coefficients of FH are close to those of FL for the *ter* locus, suggesting paired sister *ter* regions are not more condensed than single ones. Inactivation of MatP significantly increased α of Ter4 FH but not the deletion of its last 20 residues or of *zapB* (Fig. 3). We suspect this effect is due to a defect of MukB exclusion from *ter* in the Δ(*matP*) strain, which would be consistent with MukB promoting long distance interaction between chromosome loci as recently proposed [13]. FH of the *ter* locus also showed lower L_c and D_c and higher K_c than FL, consistent with their very low mobility and high constraint. Surprisingly, this is only partly suppressed by mutation of *matP* (compare Fig. 2 and 3) and even less by *matPΔ20* or mutation of *zapB* (Fig. 3). These results are consistent with the low mobility of FH of the *ter* locus being primarily due to the post-replicative pairing of sister *ter* regions. In this view, the role of MatP is to delay the separation of sister *ter* regions, hence the drastic effect of *matP* mutation on the frequency of FH, but only marginally to constrain their mobility *per se*.

Different activities of MatP, dependent and independent of its 20 last residues, are involved in the formation and/or maintenance of highly fluorescent foci (FH) at the *ter* locus (Fig. 3a). Assuming FH contain paired sister loci (see above), at least two MatP activities are involved in this pairing. We suspect that the activity remaining in the *matPΔ20* strain involves the control of sister chromosome decatenation. Indeed, inhibition of decatenation hinders sister chromosome separation [43–47] and MatP may control the activity of TopoIV, the main *E. coli* decatenase, by several mechanisms. First, MatP interacts with MukB, which in turn interacts with TopoIV [15,48,49]. It is proposed that MatP excludes TopoIV from *ter* by excluding MukB [15]. Second, catalysis by TopoIV at the *dif* site decreases in a Δ(*matP*) strain [11]. Third, FtsK, which also interacts with and activate TopoIV [50,51], acts to segregate sister *ter* regions in a MatP-dependent manner [10]. On the other hand, the functions of MatP depending on its 20 last residues certainly involve the formation of MatP tetramers and the interaction of MatP with ZapB. Indeed, most of the effect of the *matPΔ20* mutation on FH formation and maintenance depends on *zapB* (Fig. 3). The link between the *ter* region and the divisome via ZapB and ZapA (the *ter*-linkage) thus appears required for the maintenance of a normal pairing of the *ter* regions. This suggests that either the *ter*-linkage also acts to maintain catenation links or that the pairing of sister *ter* regions is partly independent of their catenation. Lastly, a small but significant part of the MatP activity dependent of its 20 last residues is independent on ZapB (Fig. 3). Thus,

either the 20 last residues of MatP participate in an undescribed activity of MatP or MatP tetramerisation plays some role in the pairing of *ter* independently of either MukB or ZapB.

We further characterized the interaction of MatP with DNA and its tetramerisation. Our data are fully consistent with MatP forming tetramers when it interacts with *matS*-containing DNA, as previously reported [12]. These DNA-bound tetramers are the major form observed in EMSA gels (Fig. S7). However, despite dedicated experiments, we were unable to detect two DNA fragments associated within these tetramers, strongly suggesting MatP tetramers contain a single *matS*-containing DNA. We detected MatP-dependent pairing of DNA molecules *in vitro* in two assays. However, this pairing activity poorly depended on the presence of *matS* sites on the DNA and was readily challenged by non-specific DNA (Fig. 4 and 5). We conclude that *matS-matS* looping or bridging by MatP is unlikely to occur frequently or stably *in vivo*, consistent with their absence in contact maps of the *E. coli* chromosome [13]. MatP tetramers may instead pair *matS* site with non-specific DNA, ensuring a part of *ter* pairing this way. This however should also lead to compaction of the *ter* region, which is argued against by the absence of anomalous component modification in Δ(*matP*) compared to wt (Fig. 3). In addition, chromatin immunoprecipitation of MatP did not reveal non-specific binding of MatP around *matS* sites [13]. We thus favor a model into which MatP tetramers bond to a *matS*-containing DNA specifically interact with ZapB, excluding other binding activity, so that the DNA-bridging activity of MatP would be observed only when ZapB is absent.

Taken together, our data support the view that MatP mainly acts to pair sister *ter* regions and to maintain this pairing until the onset of cell division, but has little effect on their dynamics when unpaired. To do so, tetramers of MatP bind *matS* sites and act in at least two ways, which can be genetically separated. This globally results in delaying decatenation by TopoIV until FtsK gets activated [52–55] and segregate the paired *ter* regions by promoting both decatenation and dimer resolution at the *dif* site [10,11].

Material and methods

Strains, media, plasmids

E. coli strains were all derived from MG1655 and provided by O. Espeli [20]. Briefly, *parS* sequences were inserted at positions 4197685bp for Ori2 locus (*parS*-P1 and *parS*-pMT1), 1395706bp for Ter3 (*parS*-P1), and 1444252bp for Ter4 (*parS*-pMT1) loci. Strains carrying a *parS*-P1 sequence were transformed with pALA2705, and strains carrying *parS*-pMT1 were transformed with pFHC2973 [27,30]. The □(*matP*) and □(*zapB*) deletions were transferred by P1 transduction from strains JW939 and JW3899 of the Keio collection [56]. The □(*matP*)$_{20}$ was obtained from F. Boccard [12]. Ampicillin (50µg/mL), Kanamycin (25µg/mL) and chloramphenicol (10µg/mL) were added when needed.

Microscopy measurements

Strains were grown at 30°C in M9 broth (Difco) supplemented with complementary salts (Mg_2SO_4 2mM, $CaCl_2$ 100µM, tryptophan 4µg/mL and Thymidine 5µg/mL), glucose and CAA (0.4% glucose, 0.1% CAA) for 6h, then diluted 2000x in M9-glucose. ParB fusion proteins production was induced for 30 min with 30µM IPTG. Cells were then deposited on a 1.5% agar pad in M9-glucose, incubated for 2h30 (2 cell cycles) at 30°C, and imaged at an $OD_{600nm} \approx 0.1$. A control experiment was done with fixed cells, which were grown as above, centrifuged, resuspended in a solution of 2% paraformaldehyde in PBS (Bioclear), incubated at 4 ˚C for 30 min and imaged as follows (Fig S10).
Imaging was done as previously described [26]. Briefly, movies were taken on a Nikon Eclipse TiE with a 60x oil-immersion objective; the images were further magnified with a 2.5x TV adapter before detection on an Andor iXon EM-CCD camera. Imaging was done at 2fps with a 0.1s exposure, for 20s to avoid photobleaching.

Image analysis and loci tracking

We achieved high precision localization of foci on each frame by two-dimensional fitting of a Gaussian function to the diffraction limited intensity distributions of individual loci [26]. This has a higher precision than typical displacements between successive frames. Particle tracks can then be obtained by matching the nearest objects in successive frames. The center of mass motion of all the common loci in the image pair is subtracted, to remove collective motion related to microscope vibration. Loci have a distribution of initial intensity, and undergo photobleaching. Tracks were analyzed using a custom written Matlab script, as previously described [26]. This was further adapted for the shorter trajectories of 40 images in our experiments. Briefly, the tracking consists of three main steps: 1) Localization of candidate particles. The aim of this step is to obtain an estimate of the particle localization; 2) Subpixel resolution detection of the position. Using the original unprocessed images, the regions around the candidate particles are fitted to a 2D Gaussian; 3) Linking of the

trajectories. In this step, the positions detected along the different time frames are assembled to reconstruct the particles trajectories.

Analysis of trajectories to extract the parameters α, L_c, D_c and K_c

The parameters have been described by Amitai and coworkers [32], and they were extracted using the same algorithm (accessible at http://bionewmetrics.org/ ; "Nuclear Organization" section). These parameters provide independent, complementary information on first and second moment statistics.

i) **The length of constraint L_c** is defined as the standard deviation (SD) of the locus position with respect to its mean averaged over time. This parameter provides estimation for the apparent radius of the volume explored by a finite trajectory. For a trajectory containing N_p points, where $\mathbf{R}_c(k\Delta t)$ is the position of a locus at a time t, L_C is obtained from the empirical estimation (1):

$$L_C = \sqrt{\mathrm{Var}(\mathbf{R}_c)} \approx \sqrt{\frac{1}{N_p}\sum_{k=1}^{N_p}(\mathbf{R}_c(k\Delta t) - \langle \mathbf{R}_c \rangle)^2}.$$

It characterises the confinement of a locus, which in other studies has been reported as the radius of confinement (R_{conf} – not to be confused with R_c). The R_{conf} is computed from the asymptotic plateau of a Mean Square Displacement (MSD) curve, and is therefore limited to trajectories that plateau. This is strongly influenced by the length of image acquisition. The advantage of computing L_C is that it gives a robust estimate of the volume $V = 4/3\pi L_C^3$ occupied by the trajectory and can be used on any kind of trajectory, as it does not require a plateau.

$$C(t) = \left\langle (\mathbf{R}_c(\tau + t) - \mathbf{R}_c(\tau))^2 \right\rangle \approx t^{\alpha}$$

ii) **The anomalous exponent α** is computed from the MSD behavior for small increments. α was estimated by fitting the first 6 points of the MSD of an SPT by a power law t^{α}.

iii) **The effective spring coefficient K_c**. The spring force acting at position x_a and measured at position x_m is represented by $F=-K_c(x_m-x_a)$. The spring constant Kc allows us to estimate the effect of local tethering interactions around the locus of interest [57]. This tethering can arise from interactions of the locus with other chromosomes or cellular substructures, such as the membrane. These interactions cannot be measured directly but they can be inferred from SPTs.

iv) **The effective diffusion coefficient D_c** reflects the second order statistical properties of a trajectory. This diffusion coefficient accounts for local crowding that may vary along the trajectory.

Calibration of the foci

In order to estimate the copy number of fluorophores, we implemented a custom intensity calibration method in MATLAB, based on the principle described in [58]. The calibration method aims at estimating the ratio between the intensity of foci and the number of GFP molecules by exploiting the intrinsic fluctuations of intensity generated by the random photobleaching process. The key idea is that the variance of the intensity drop depends on the number of emitting GFP molecules contained in the

focus at the beginning of acquisition. I.e.: a higher number of emitting GFP molecules corresponds to a smaller variance in the relative intensity loss (see Supplementary Materials for the detailed calculation and algorithm). We estimate the intensity/copy number ratio (calibration ratio) by binning the foci by initial intensity, and evaluating the dependence of the variance of the intensity drop on the bin.

Statistics

Distributions are plotted using the boxplot script in Matlab, therefore showing the median of the distribution (horizontal line), the 25th and 75th percentiles of the samples (respectively the bottom and top of the box), the lowest and top values within a range of 1.5 times the interquartile range (dotted lines), and outliers of these as crosses. The notches display the variability of the median; non-overlapping notches between samples indicate different value of the medians at a 5% significance level. Each strain was tested at least 3 times independently, and the data were pooled in the same data file. The final numbers of foci used for data analysis are indicated in Table S1. Table S2 shows the median for each dataset.

To compare distributions, a two-sample Kolmogorov–Smirnov test was used and p values are indicated in the text and Table S3. Unless stated, the distributions of foci at midcell (M) were used to compare 2 strains or type of foci (FH or FL).

MatP purification

A pET15b containing *matP* or *matPΔ20* was transformed into BL21 cells. After 2h induction with 1mM IPTG, cells were centrifuged and pellets were resuspended in RB1 (20mM Tris pH7.5, 300mM NaCl, 1mM DTT, 5% glycerol and protease inhibitor (complete EDTA-Free, Roche)). Cells were lysed by sonication, centrifuged and resuspended in RB1 for a step of ultra-centrifugation (50000rpm for 90min at 4°C). The supernatant was loaded onto a heparin column (Hitrap Heparin HP, GE Healthcare Life Sciences) and MatP was eluted with a NaCl gradient (0.3 to 1M) in RB1 with 5mM $MgCl_2$. MatP fractions were pooled, dialysed (20mM Tris pH7.5, 250mM NaCl, 1mM DTT, 5mM $MgCl_2$, 20% glycerol) and frozen.

His-tagged MatPΔ20 was cloned and expressed as above; after the first centrifugation, it was loaded onto a HisTrap column (HisTrap, GE Healthcare Life Sciences) and eluted with an imidazole gradient (0 to 0.5M; 10 column volumes). MatPΔ20 fractions were pooled, dialysed (20mM Tris pH 7.5, 250mM NaCl, 1mM DTT, 2mM EDTA, 10% glycerol) and frozen.

Pull-down experiments

Magnetic beads (1µL/reaction, Streptavidine MagneSphere® Paramagnetic Particles, Promega) were washed twice in PBS and once in RB2 (20mM Tris pH7.5, 1mM $MgCl_2$, 150mM NaCl, 1mg/mL BSA), then resuspended in RB2. Biotinylated DNA_b (10ng) ($DNA_{b(2matS)}$: 3746pb, $DNA_{b(1matS)}$: 3800pb, $DNA_{b(0matS)}$: 3700pb) was added and incubated at RT for 30min. The DNA-bead complexes were

then washed and resuspended in RB2, and the non-biotinylated, DNA_f (20ng) was added ($DNA_{f(2matS)}$: 1701pb, $DNA_{f(1matS)}$: 1717pb, $DNA_{f(0matS)}$: 1688pb), along with 100nM competitor DNA (25bp, double-stranded, non-specific oligo). Finally, MatP (respectively 0,0.1,0.2,0.5,1 and 2µM) was added and reactions were incubated for 15min at RT. After this time, the supernatant was removed and reactions were quickly washed with 15µL RB2, then resuspended in 15µL RB2 + 0.1% SDS. After 10min, the supernatant was deposited on a 0.8% agarose gel. DNA was visualized with Sybr-Green (Life technologies).

Multiplexed tethered particle motion (TPM)

The overall TPM procedure, including data analysis, has been described previously [37,59]. The complexed beads-DNA (2284bp) were incubated O/N in the chambers at 4°C in RB3 (PBS 1X, 5mg/mL Pluronic F-127, 0.1mg/mL BSA, 0.1% SDS and 0.05% Triton 100X) and the free beads were washed with RB3. Chambers were then washed with RB4 (20mM Tris pH7.5, 1mM $MgCl_2$, 150mM NaCl, 0.1mg/ml BSA, 5mg/mL Pluronic F-127), and imaged for 2min before injection of 600nM MatP or MatPΔ20. Traces were examined one by one as described in [39]. Only those with an appropriate amplitude of motion measured in absence of proteins, regarding the calibration curve, were conserved for further analysis. We analyzed the kinetics of the amplitude of motion after 5 min after injection of proteins and used for that detection methods based on thresholds defined as midways between the peak positions found in the histograms of amplitude of motion. We thus defined 2 states: state 1, intact DNA, and state 2, apparently looped DNA and detected them on each trace. The histograms of the state duration were fitted with 2 exponential decays leading to $\boldsymbol{\tau}_{fast}$ and $\boldsymbol{\tau}_{slow}$.

Electromobility shift assays (EMSA)

The *matS41* DNA (41 bp) was obtained by hybridizing oligonucleotides matS41top (5'-CY3-AAGTACGGTAAAAGGTGACAGTGTCACTTTCATTGTTGGTA) and matS41bottom (5'-TAC-CAACAATGAAAGTGACACTGTCACCTTTTACCGTACTT). The *matS237* DNA (237 bp) was obtained by PCR amplification using pEL3, a pLN135 derivative containing the *matS* sequence (our lab collection: *matS* site: GTGACAGTGTCAC), as a matrix and FmatS (5'-GTAGTGCCGGGA-GAAAGCAG) and RmatS (5'-GCCTTCTTGACGAGTTCTTC) as oligonucleotides. Binding reactions were done in buffer containing 10mM Tris (pH 7.5), 125 mM NaCl, 2.5 mM MgCl2, 0.5mM DTT, and 5% glycerol, in the presence of 1µM of each DNA probe, 0.25 µg of poly(dI-dC) and different concentrations of indicated proteins (4µM of proteins in Figure 6 and 3µM and 6µM in figure S8) The reactions were incubated at 30°C for 30 min and analyzed on 5% native TGE PAGE.

References

1. Joyeux, M. Compaction of bacterial genomic DNA: clarifying the concepts. *J Phys Condens Matter* **27**, 383001 (2015).
2. Wang, X. & Rudner, D. Z. Spatial organization of bacterial chromosomes. *Current Opinion in Microbiology* **22**, 66–72 (2014).

3. Kleckner, N. *et al.* The Bacterial Nucleoid: Nature, Dynamics and Sister Segregation. *Curr Opin Microbiol* **22**, 127–137 (2014).
4. Marbouty, M. *et al.* Condensin- and Replication-Mediated Bacterial Chromosome Folding and Origin Condensation Revealed by Hi-C and Super-resolution Imaging. *Molecular Cell* **59**, 588–602 (2015).
5. Niki, H., Yamaichi, Y. & Hiraga, S. Dynamic organization of chromosomal DNA in Escherichia coli. *Genes Dev.* **14**, 212–223 (2000).
6. Umbarger, M. A. *et al.* The Three-Dimensional Architecture of a Bacterial Genome. *Mol Cell* **44**, (2011).
7. Valens, M., Penaud, S., Rossignol, M., Cornet, F. & Boccard, F. Macrodomain organization of the Escherichia coli chromosome. *EMBO J.* **23**, 4330–4341 (2004).
8. Vallet-Gely, I. & Boccard, F. Chromosomal Organization and Segregation in Pseudomonas aeruginosa. *PLoS Genet* **9**, (2013).
9. Mercier, R. *et al.* The MatP/matS Site-Specific System Organizes the Terminus Region of the E. coli Chromosome into a Macrodomain. *Cell* **135**, 475–485 (2008).
10. Stouf, M., Meile, J.-C. & Cornet, F. FtsK actively segregates sister chromosomes in Escherichia coli. *Proc. Natl. Acad. Sci. U.S.A.* **110**, 11157–11162 (2013).
11. El Sayyed, H. *et al.* Mapping Topoisomerase IV Binding and Activity Sites on the E. coli Genome. *PLoS Genet* **12**, (2016).
12. Dupaigne, P. *et al.* Molecular Basis for a Protein-Mediated DNA-Bridging Mechanism that Functions in Condensation of the E. coli Chromosome. *Molecular Cell* **48**, 560–571 (2012).
13. Lioy, V. S. *et al.* Multiscale Structuring of the E. coli Chromosome by Nucleoid-Associated and Condensin Proteins. *Cell* (2017). doi:10.1016/j.cell.2017.12.027
14. Espéli, O. *et al.* A MatP–divisome interaction coordinates chromosome segregation with cell division in E. coli. *EMBO J* **31**, 3198–3211 (2012).
15. Nolivos, S. *et al.* MatP regulates the coordinated action of topoisomerase IV and MukBEF in chromosome segregation. *Nat Commun* **7**, 10466 (2016).
16. Buss, J. *et al.* A Multi-layered Protein Network Stabilizes the Escherichia coli FtsZ-ring and Modulates Constriction Dynamics. *PLoS Genet* **11**, e1005128 (2015).
17. Bailey, M. W., Bisicchia, P., Warren, B. T., Sherratt, D. J. & Männik, J. Evidence for Divisome Localization Mechanisms Independent of the Min System and SlmA in Escherichia coli. *PLoS Genet* **10**, (2014).
18. Cass, J. A., Kuwada, N. J., Traxler, B. & Wiggins, P. A. Escherichia coli Chromosomal Loci Segregate from Midcell with Universal Dynamics. *Biophysical Journal* **110**, 2597–2609 (2016).
19. Elmore, S., Müller, M., Vischer, N., Odijk, T. & Woldringh, C. L. Single-particle tracking of oriC-GFP fluorescent spots during chromosome segregation in Escherichia coli. *Journal of Structural Biology* **151**, 275–287 (2005).
20. Espeli, O., Mercier, R. & Boccard, F. DNA dynamics vary according to macrodomain topography in the E. coli chromosome. *Molecular Microbiology* **68**, 1418–1427 (2008).
21. Fisher, J. K. *et al.* Four dimensional imaging of E. coli nucleoid organization and dynamics in living cells. *Cell* **153**, 882–895 (2013).
22. Javer, A. *et al.* Persistent super-diffusive motion of Escherichia coli chromosomal loci. *Nat Commun* **5**, (2014).
23. Kuwada, N. J., Cheveralls, K. C., Traxler, B. & Wiggins, P. A. Mapping the driving forces of chromosome structure and segregation in Escherichia coli. *Nucleic Acids Res* **41**, 7370–7377 (2013).
24. Fiebig, A., Keren, K. & Theriot, J. A. Fine-scale time-lapse analysis of the biphasic, dynamic behaviour of the two Vibrio cholerae chromosomes. *Mol Microbiol* **60**, 1164–1178 (2006).
25. Weber, S. C., Spakowitz, A. J. & Theriot, J. A. Bacterial Chromosomal Loci Move Subdiffusively through a Viscoelastic Cytoplasm. *Phys Rev Lett* **104**, 238102 (2010).
26. Javer, A. *et al.* Short-time movement of *E. coli* chromosomal loci depends on coordinate and subcellular localization. *Nature Communications* **4**, ncomms3003 (2013).
27. Nielsen, H. J., Ottesen, J. R., Youngren, B., Austin, S. J. & Hansen, F. G. The Escherichia coli chromosome is organized with the left and right chromosome arms in separate cell halves. *Molecular Microbiology* **62**, 331–338 (2006).
28. Bates, D. & Kleckner, N. Chromosome and Replisome Dynamics in E. coli: Loss of Sister Cohesion Triggers Global Chromosome Movement and Mediates Chromosome Segregation. *Cell*

121, 899–911 (2005).
29. Wang, X., Possoz, C. & Sherratt, D. J. Dancing around the divisome: asymmetric chromosome segregation in Escherichia coli. *Genes Dev.* **19**, 2367–2377 (2005).
30. Nielsen, H. J., Li, Y., Youngren, B., Hansen, F. G. & Austin, S. Progressive segregation of the Escherichia coli chromosome. *Molecular Microbiology* **61**, 383–393 (2006).
31. Mercier, R. *et al.* The MatP/matS Site-Specific System Organizes the Terminus Region of the E. coli Chromosome into a Macrodomain. *Cell* **135**, 475–485 (2008).
32. Amitai, A., Seeber, A., Gasser, S. M. & Holcman, D. Visualization of Chromatin Decompaction and Break Site Extrusion as Predicted by Statistical Polymer Modeling of Single-Locus Trajectories. *Cell Reports* **18**, 1200–1214 (2017).
33. Shukron, O. & Holcman, D. Statistics of randomly cross-linked polymer models to interpret chromatin conformation capture data. *Phys Rev E* **96**, 012503 (2017).
34. Shukron, O., Seeber, A., Amitai, A. & Holcman, D. Advances Using Single-Particle Trajectories to Reconstruct Chromatin Organization and Dynamics. *Trends Genet.* **35**, 685–705 (2019).
35. Wlodarski, M. *et al.* Both genome and cytosol dynamics change in E. coli challenged with sublethal rifampicin. *Phys. Biol.* **14**, 015005 (2017).
36. Ebersbach, G., Galli, E., Møller-Jensen, J., Löwe, J. & Gerdes, K. Novel coiled-coil cell division factor ZapB stimulates Z ring assembly and cell division. *Molecular Microbiology* **68**, 720–735 (2008).
37. Plénat, T., Tardin, C., Rousseau, P. & Salomé, L. High-throughput single-molecule analysis of DNA-protein interactions by tethered particle motion. *Nucleic Acids Res.* **40**, e89 (2012).
38. Manghi, M. *et al.* Probing DNA conformational changes with high temporal resolution by tethered particle motion. *Phys Biol* **7**, 046003 (2010).
39. Diagne, C. T. *et al.* TPM analyses reveal that FtsK contributes both to the assembly and the activation of the XerCD-dif recombination synapse. *Nucl. Acids Res.* **42**, 1721–1732 (2014).
40. Fournes, F. *et al.* FtsK translocation permits discrimination between an endogenous and an imported Xer/dif recombination complex. *PNAS* 201523178 (2016). doi:10.1073/pnas.1523178113
41. Wu, F. *et al.* Cell Boundary Confinement Sets the Size and Position of the E. coli Chromosome. *Current Biology* **29**, 2131-2144.e4 (2019).
42. Lesterlin, C., Pages, C., Dubarry, N., Dasgupta, S. & Cornet, F. Asymmetry of chromosome Replichores renders the DNA translocase activity of FtsK essential for cell division and cell shape maintenance in Escherichia coli. *PLoS Genet.* **4**, e1000288 (2008).
43. Adams, D. E., Shekhtman, E. M., Zechiedrich, E. L., Schmid, M. B. & Cozzarelli, N. R. The role of topoisomerase IV in partitioning bacterial replicons and the structure of catenated intermediates in DNA replication. *Cell* **71**, 277–288 (1992).
44. Steck, T. R. & Drlica, K. Bacterial chromosome segregation: evidence for DNA gyrase involvement in decatenation. *Cell* **36**, 1081–1088 (1984).
45. Wang, X., Reyes-Lamothe, R. & Sherratt, D. J. Modulation of Escherichia coli sister chromosome cohesion by topoisomerase IV. *Genes Dev* **22**, 2426–2433 (2008).
46. Joshi, M. C. *et al.* Regulation of Sister Chromosome Cohesion by the Replication Fork Tracking Protein SeqA. *PLoS Genet* **9**, (2013).
47. Lesterlin, C., Gigant, E., Boccard, F. & Espéli, O. Sister chromatid interactions in bacteria revealed by a site-specific recombination assay. *EMBO J* **31**, 3468–3479 (2012).
48. Hayama, R. & Marians, K. J. Physical and functional interaction between the condensin MukB and the decatenase topoisomerase IV in Escherichia coli. *Proc Natl Acad Sci U S A* **107**, 18826–18831 (2010).
49. Vos, S. M., Stewart, N. K., Oakley, M. G. & Berger, J. M. Structural basis for the MukB-topoisomerase IV interaction and its functional implications in vivo. *EMBO J* **32**, 2950–2962 (2013).
50. Espeli, O., Lee, C. & Marians, K. J. A Physical and Functional Interaction between Escherichia coli FtsK and Topoisomerase IV. *J. Biol. Chem.* **278**, 44639–44644 (2003).
51. Bigot, S. & Marians, K. J. DNA chirality-dependent stimulation of topoisomerase IV activity by the C-terminal AAA+ domain of FtsK. *Nucleic Acids Res* **38**, 3031–3040 (2010).
52. Steiner, W. W. & Kuempel, P. L. Cell division is required for resolution of dimer chromosomes at the dif locus of Escherichia coli. *Mol. Microbiol.* **27**, 257–268 (1998).
53. Steiner, W., Liu, G., Donachie, W. D. & Kuempel, P. The cytoplasmic domain of FtsK protein is

required for resolution of chromosome dimers. *Mol. Microbiol.* **31**, 579–583 (1999).
54. Kennedy, S. P., Chevalier, F. & Barre, F.-X. Delayed activation of Xer recombination at dif by FtsK during septum assembly in Escherichia coli. *Mol. Microbiol.* **68**, 1018–1028 (2008).
55. Bisicchia, P., Steel, B., Debela, M. H. M., Löwe, J. & Sherratt, D. The N-Terminal Membrane-Spanning Domain of the Escherichia coli DNA Translocase FtsK Hexamerizes at Midcell. *mBio* **4**, e00800-13 (2013).
56. Baba, T. *et al.* Construction of Escherichia coli K-12 in-frame, single-gene knockout mutants: the Keio collection. *Mol Syst Biol* **2**, 2006.0008 (2006).
57. Amitai, A., Toulouze, M., Dubrana, K. & Holcman, D. Analysis of Single Locus Trajectories for Extracting In Vivo Chromatin Tethering Interactions. *PLoS Comput. Biol.* **11**, e1004433 (2015).
58. Nayak, C. R. & Rutenberg, A. D. Quantification of Fluorophore Copy Number from Intrinsic Fluctuations during Fluorescence Photobleaching. *Biophysical Journal* **101**, 2284–2293 (2011).
59. Brunet, A. *et al.* Probing a label-free local bend in DNA by single molecule tethered particle motion. *Nucleic Acids Res.* **43**, e72 (2015).

Acknowledgements
We would like to thank M. Consentino-Lagomarsino, A. Javer, J. Kotar, M. Wlodarski, M. Panlilio for helpful discussions and help with softwares and microscopy experiments. We are also grateful to F. Boccard and O. Espeli for the kind gifts of bacterial strains and plasmids.
Research in the FC group is founded by the CNRS and the Université Paul Sabatier (UPS Toulouse). Research in PC lab was founded by an HFSP grant to PC and BS.

Author contributions
EC, PR, PC and FC conceived the project. EC performed the microscopy experiments. EC, DH, BS and PC discussed the microscopy results. EC, CT and MS performed the TPM experiments. EC, MS, PR and AL performed the biochemical experiments. TB performed the foci calibrations. EC, PR, PC and FC wrote the manuscript. All authors discussed the results and commented on the manuscript.

Competing interests
The authors declare no competing interests.

Supplementary Material

1. Detailed calculation for the calibration of foci

Given a focus with n emitting molecules, the observed intensity will be

$$I = \nu n$$

Here we aim at estimating the calibration ratio ν from the fluctuations in the intensity drop due to photobleaching.

At any given time t, the number of emitting GFP molecules in a focus with n_0 initial emitting molecules, is described by a binomial distribution with $n=n_0$, and $p=e^{\frac{-t}{\tau}}$ where τ is the bleaching time constant. The variance of the binomial distribution is given by

$$Var(\Delta n) = n_0 p(1-p)$$

Where Δn represents the number of bleached molecules, and p the probability of bleaching until time t. Then the contribution of bleaching to the variance of the intensity drop is:

$$Var(\Delta I)_b = \nu^2 n_0 p(1-p) = \nu I_0 p(1-p)$$

Where ΔI represents the total intensity loss for a given focus and the subscript b indicates that the term is relative to the component of variance coming from fluctuations in the bleaching process.

This establishes a linear relationship between the variance of the intensity drop and the calibration ratio, that can be estimated as the slope of $Var(\Delta I)_b$ as a function of $I_0 p(1-p)$ on a linear fit (with intercept constrained at 0) on several initial intensity bins (Fig. S3C). P is estimated from the data through a fit on ΔI as a function of I_0 (Fig. S3A). This also allows to estimate the bleaching time constant τ that will be used in the following steps.

In order to estimate the contribution of bleaching to the total intensity variance, we model it as follows:

$$Var(\Delta I)_{total} = Var(\Delta I)_b + Var(\Delta I)_{other} = \nu I_0 p(1-p) + \gamma I$$

Where γI groups non-bleaching variance contributions such as shot noise, and is expected to be proportional to intensity.

Since we expect $p(t) = e^{\frac{-t}{\tau}}$ and $I(t) = I_0 e^{\frac{-t}{\tau}}$ we can substitute it in the above equation and fit the following expression to the observed variance as a function of time (Fig. S3B):

$$Var(\Delta I)_{total} = \gamma e^{\frac{-t}{\tau}} + \nu I_0 \left(e^{\frac{-t}{\tau}} - e^{-2\frac{t}{\tau}} \right)$$

The bleaching dependent part of variance (the second term of the expression) has a different functional dependence on time, and therefore can be disentangled from other sources of variance and used to estimate the calibration parameter through the above described linear fitting. This process

also allowed to verify that the bleaching contribution is indeed the dominant contribution in the empirical variance. As an additional pre-processing step, we estimate and subtract background intensity by extrapolating the intensity at which no bleaching is observed (Fig. S3A).

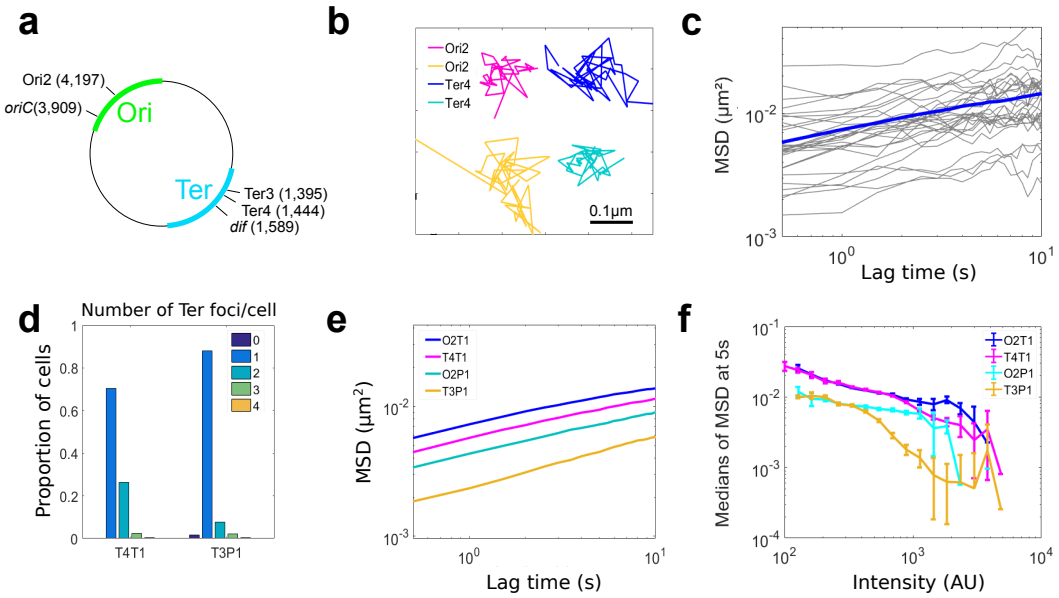

Figure 1. The type of visualisation system affects the mobility of chromosomal loci

a Scheme of *E. coli* chromosome showing two macrodomains, the origin of replication *oriC* and the site-specific recombination site *dif*, plus the loci where *parS* sites have been inserted, called Ori2, Ter3 and Ter4. Positions are indicated in Mbp. **b** Examples of tracks for Ori2 and Ter4 loci; 2fps for 20s. **c** Example of 30 MSD from Ter4 (parB-pMT1) locus as a function of lagtime (grey lines), with the median for all MSD of this experiment (n=1600) shown in blue. **d** Number of Ter foci per cell (dark blue, cells with no focus; orange, cells with 4 foci), with ParB-P1 (T3P1) or parB-pMT1 (T4T1). Y axe represents the proportion of cells with that number of foci compared to the total number of cells. **e** Medians of MSDs as a function of lagtime for Ori2-ParB-P1 (O2P1), Ori2-ParB-pMT1 (O2T1), Ter3-ParB-P1 (T3P1) and Ter4-ParB-pMT1 (T4P1). **f** MSD of ParB-P1 and ParB-pMT1 foci at 5s as a function of intensity of the foci. Error bars show the SEM (Standard error of the mean).

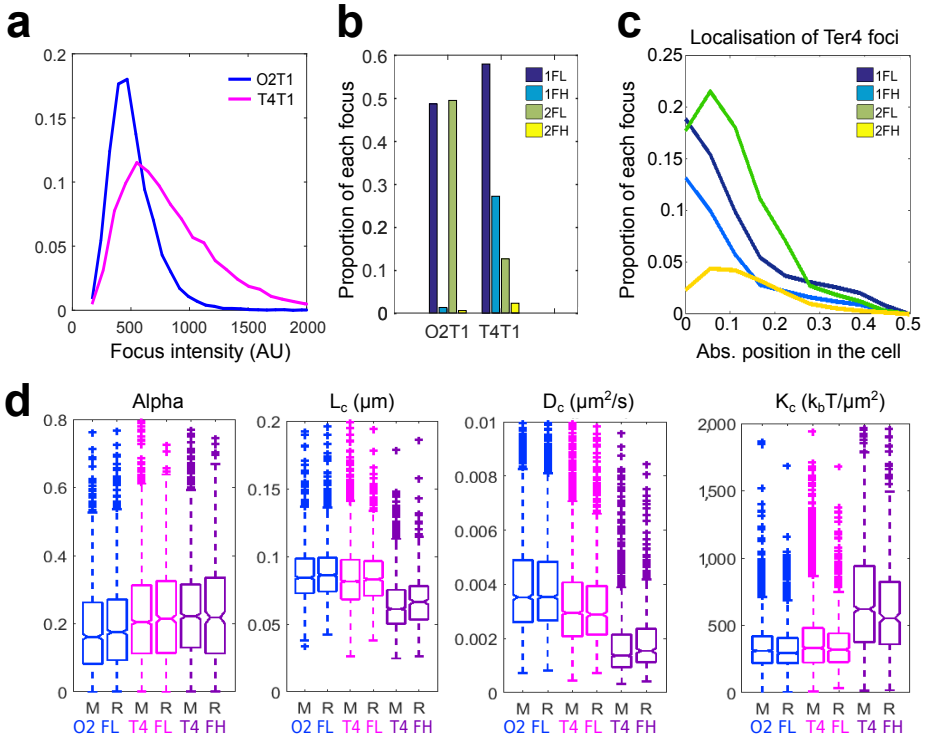

Figure 2. The high intensity Ter4 foci display a slower dynamics.

a Distribution of intensity of Ori2 and Ter4 ParS-pMT1 foci. **b** Proportion of each type of focus in Ori2 and Ter4 strains. 1FL: single, low intensity focus in the cell; 1FH: single, high intensity focus in the cell; 2FL: low intensity focus detected in a cell with 2 foci; 2FH: high intensity focus detected in a cell with 2 foci. The numbers of foci of each type are indicated in Table S1. **c** Proportion of Ter4 foci as a function of their position in the cell. 0 is midcell, while 0.5 is a cell pole **d** The four parameters α, L_c, D_c and K_c were calculated for Ori2 and Ter4 foci, which were divided in low (FL) or high intensity (FH) foci, and in foci localised at midcell (M, 0-0.16) or away from midcell (R, 0.17-0.5). Ori2 1FL (blue), Ter4 1FL (pink) and Ter4 1FH (purple) are shown. The number of 1FH for Ori2 is too low to give significant results (Table S1) and is therefore not plotted here. The values of medians are indicated in Table S2.

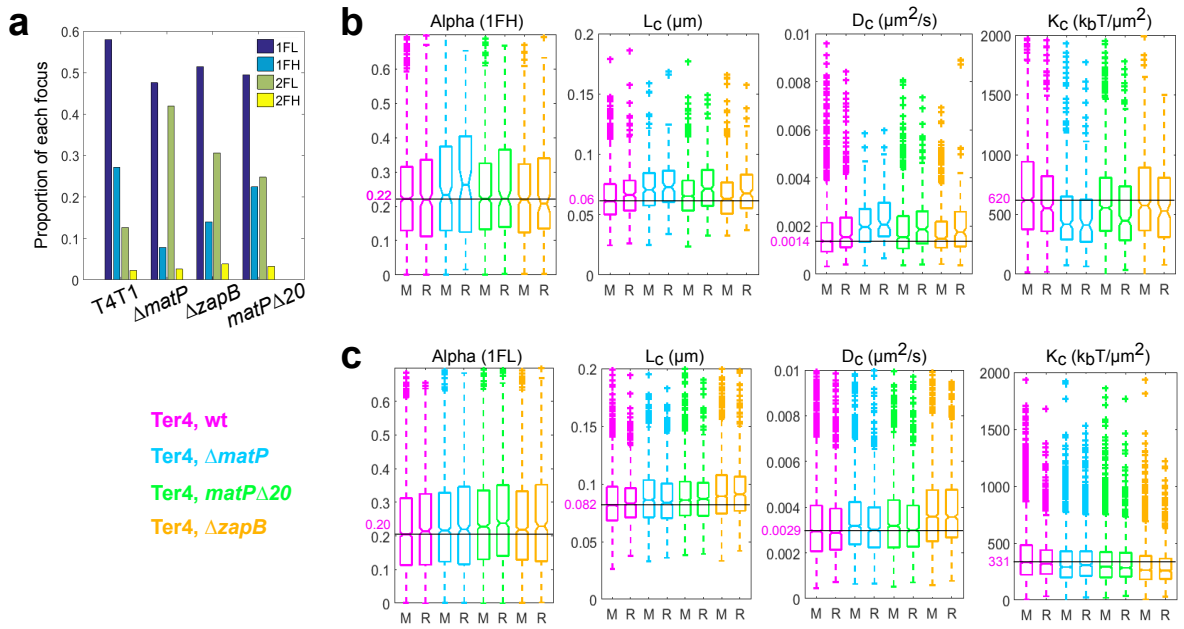

Figure 3. Ter4 foci are more mobile in *MatP* mutants.

a Proportion of each type of focus in Ter4 mutant strains. **b** - **c** The four parameters α, L_c, D_c and K_c were calculated for 1FH Ter4 foci (**b**), and 1FL Ter4 foci (**c**). Wild type (pink) and mutant backgrounds (Δ*matP*, blue; *matPΔ20*, green; Δ*zapB*, orange) are presented as in Fig. 2d. To help comparing the values, a line has been drawn at the value for the foci at midcell in the wt background, the value indicated in pink, and the outliners at high values have been cut off.

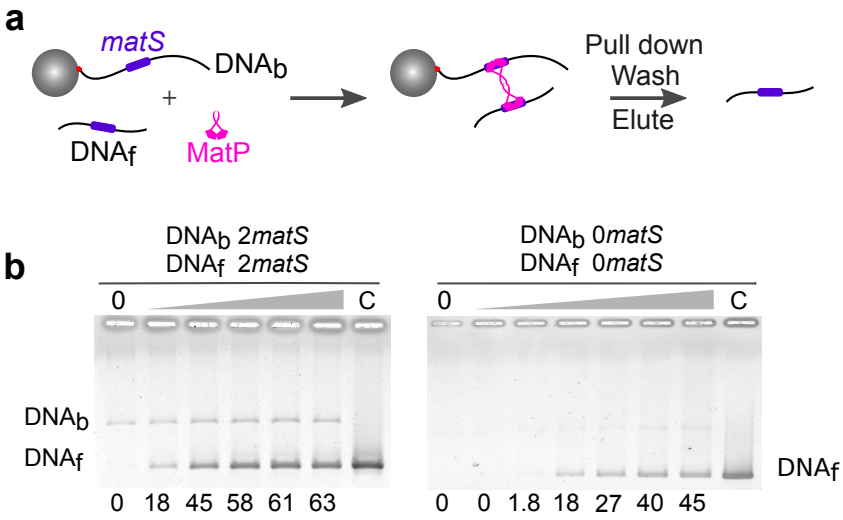

Figure 4. MatP can bridge DNA

a Scheme of the pull-down experiment. A biotinylated DNA (DNA_b) containing 0, 1 or 2 *matS*, is attached to a streptavidin-covered, magnetic bead. Free DNA (DNA_f), containing 0,1 or 2 *matS*, is added to the reaction, alongside a competitor (40bp, non-specific, double-stranded DNA). Different concentrations of MatP are added to the mix. The reactions are pulled-down a first time, rinsed with buffer, eluted with 0.1% SDS, which denatures MatP but not the streptavidin, and pulled down again. DNA_f is recovered if MatP has induced bridging. Those are then loaded on an agarose gel. **b** Examples of gels obtained with both DNA_b and DNA_f containing 2 *matS* (left) or no *matS* (right). Concentration of MatP is from left to right: 0, 0.1, 0.25, 0.5, 1 and 2µM, with an additional reaction with 4µM for the gel on the right. The percentage of recovered DNA_f is shown below each lane; lane C shows the initial amount of DNA_f (20ng). Quantitation can vary from gel to gel but the trend is the same within 3 independent experiments.

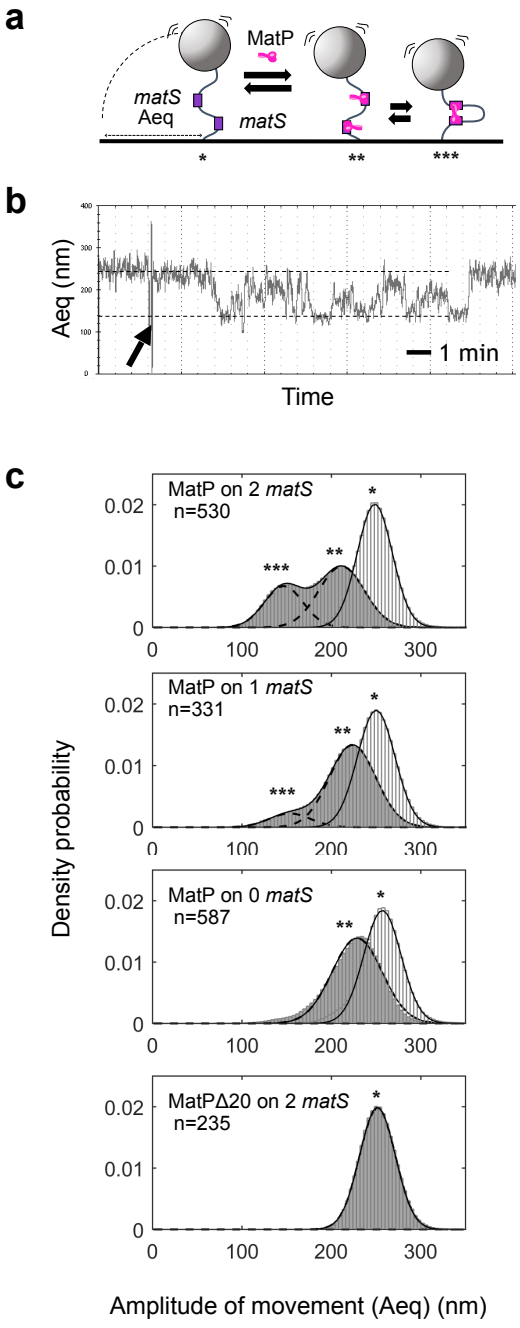

Figure 5. MatP can loop DNA

a Scheme of the TPM set-up. A glass coverslip is coated with PEG and neutravidin. A DNA molecule is attached to that surface by a biotin bound to one of its 5' end. A latex bead coated with antidigoxigenin is bound to the other extremity of the DNA molecule by the presence of digoxigenin on this 5' end. The amplitude of the Brownian motion of the bead (Aeq) depends on the size of the DNA molecule that tethers the bead to the glass surface (for details see text and M&M). Right: if MatP joins the 2 *matS* sites together, the Aeq decreases. **b** Example of a track following a bead tethered to a 2-*matS*-DNA as a function of time. The dotted lines indicate the expected Aeq for a naked DNA (top) or looped DNA (bottom). MatP is added after 2 min (arrow) and the bead tracked for another 13min. **c** Probability distributions of Aeq, before protein injection (light grey histogram), or during the 5 min following the injection (dark grey histograms). The type of DNA (0 to 2 *matS*), the type of MatP (wt or Δ20) and the number of tracks obtained for each condition are indicated on the graphs. MatP: *, population centred on (mean +/- SD, in nm) : 248 +/-19; 250 +/-21 and 257 +/-21 for the DNA containing 2, 1 and no *matS* site, respectively. **, population centred on (mean +/- SD, in nm): 211 +/- 25, 224 +/- 26 and 229 +/- 28 for the DNA containing 2, 1 and no *matS* site, respectively. ***, population centred on (mean +/- SD, in nm): 147 +/- 22 and 153 +/- 23 for the DNA containing 2 and 1 *matS* site, respectively. MatPΔ20: *, population centred on (mean +/- SD) : 252 +/- 20nm.

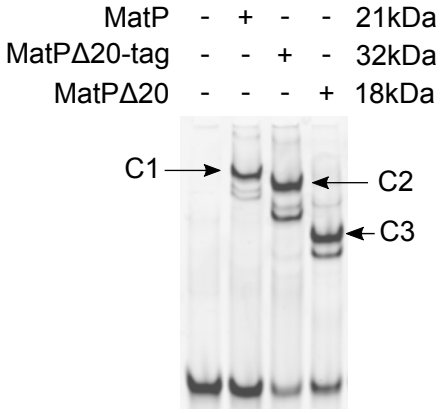

Mw_{theo} (kDa)	Hyp1	Hyp2	Hyp3
C1	69	111	111
C2	91	155	91
C3	63	99	63

Figure 6. MatP binds *matS* as a tetramer

EMSA experiment showing the interaction between a 41bp DNA fragment containing *matS* (MW_{theo}= 27kDa) and 3µM of MatP (MW_{theo}= 21kDa), his-tagged MatPΔ20 (MW_{theo}= 32kDa), or untagged MatPΔ20 (MW_{theo}= 18kDa). Based on the theoretical molecular weight (MW_{theo}) of the DNA molecule and of the different protein used, we have estimated the theoretical molecular weight of the different protein-DNA complexes following 3 different hypotheses. Hypothesis 1 (Hyp.1) proposes that MatP and MatPΔ20 binds DNA as a dimer; Hypothesis 2 (Hyp.2) proposes that MatP and MatPΔ20 binds DNA as a tetramer; Hypothesis 3 (Hyp.3) proposes that MatP binds DNA as a tetramer whereas MatPΔ20 binds DNA as a dimer. Note that only Hypothesis 3 proposes theoretical molecular weights that are in accordance with EMSA results.

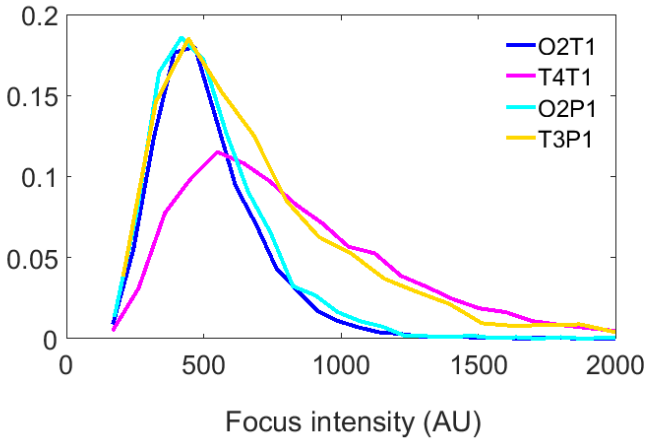

Figure S1: Intensities of foci labeled with ParS-P1 and ParS-pMT1

Distribution of intensity for Ori2 and Ter3 or Ter4 foci labeled with ParS-P1 (O2P1 and T3P1) or ParS-pMT1 (O2T1 and T4T1).

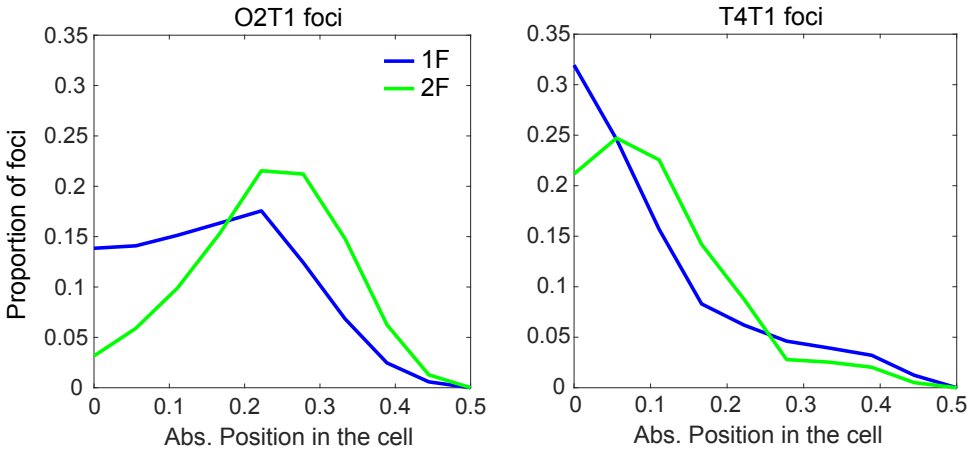

Figure S2: Cell localisation of Ori2 and Ter4 foci

Localisation of Ter4 foci in a wild-type strain as a function of foci number and their intensity.

Position in the cell is given from midcell (0) to the cell pole (0.5).

Note that only the foci that have a trajectory that has been validated by the script are plotted here, leading to an over-representation of 1F cells.

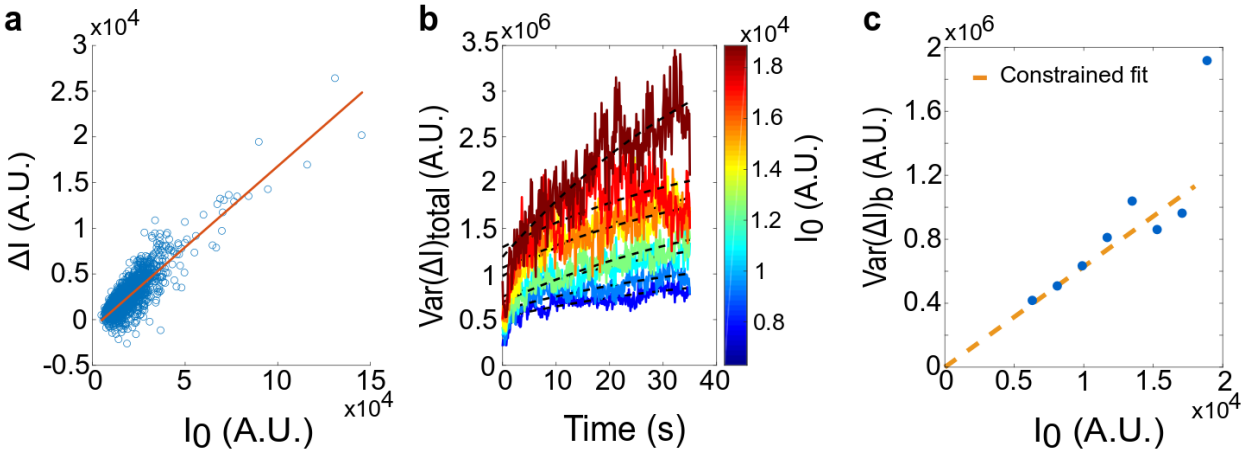

Figure S3: Calibration of intensity/copy number ratio on a sample acquisition session

a Background intensity, bleaching probability and time constant are estimated from the total intensity loss as a function of initial intensity. The estimated background intensity is subtracted before further processing. **b** Estimation of the bleaching contribution to variance over time. Tracks are binned by initial intensity, and variance in the intensity drop is computed per bin and per timepoint. Then, the variance as a function of time is fit with two terms, accounting for the bleaching and the short noise contributions to the intensity drop variance (see supplementary text for calculations). If variance was not dominated by bleaching, we would expect it to decay over time proportionally to intensity. On the graph, the bleaching term is roughly the difference between the end and the beginning of the black dashed curves. **c** The calibration parameter is estimated through a linear fit with intercept constrained to 0. The calibration parameter is obtained by dividing the slope of the linear fit by p(1-p), where p is the bleaching probability estimated in panel a.

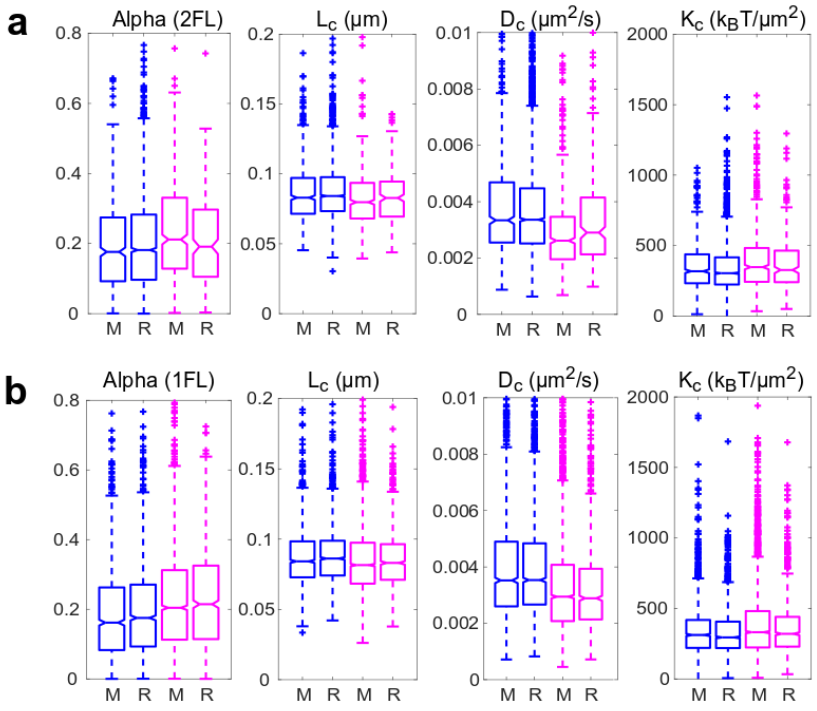

Figure S4: Mobility of 2FL in Ori2 and Ter4

The four parameters α, L_c, D_c and K_c were calculated and are plotted as in Fig. 2D for Ori2 locus (blue) and Ter4 (pink) in wt background. **a** Results for 2FL. **b** For an easier comparison, results are also shown for 1FL (same as in Fig 2D).

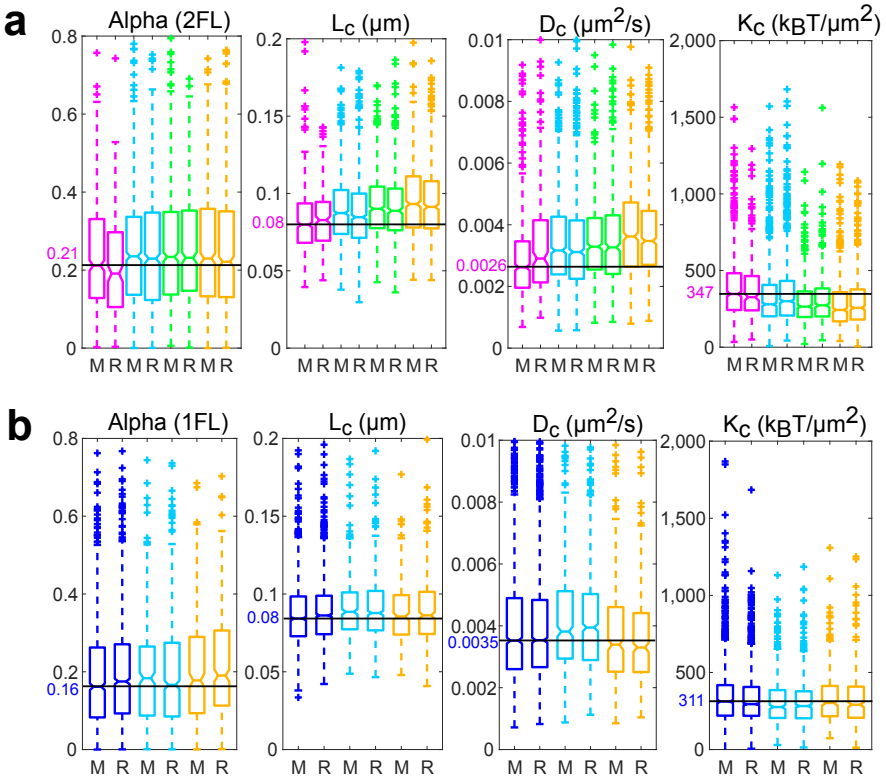

Figure S5: Mobility of 2FL foci in mutant strains

The four parameters α, L_c, D_c and K_c were calculated and are plotted as in Fig. 2d. **a** Results for 2FL for Ter4 locus in wt (pink), Δ*matP* (light blue), *matPΔ20* (green) and Δ*zapB* (orange) backgrounds. **b** Ori2 locus in wt (dark blue), Δ*matP* (light blue) and Δ*zapB* (orange) backgrounds. Results here are shown for 1FL only, the number of 1FH being too low to give relevant results (Table S1). To help comparing the values, a line has been drawn at the value for the foci at midcell in the wt background, the value indicated in pink (**a**) or blue (**b**), and the outliners at high values have been cut off.

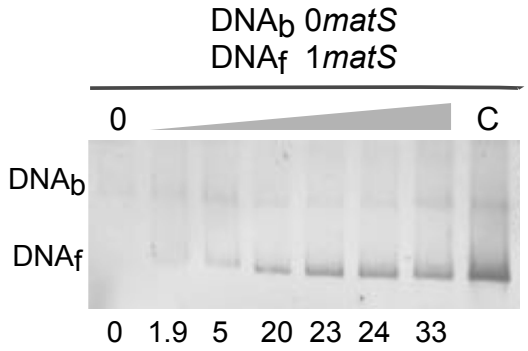

Figure S6: Pull-down experiments

The experiment is done as in Fig. 4. Here DNA_b contains no *matS*, while DNA_f contains one *matS*. Percentage of DNA recovered is indicated at the bottom of the gel. The concentration of MatP is the same as in Fig. 5.

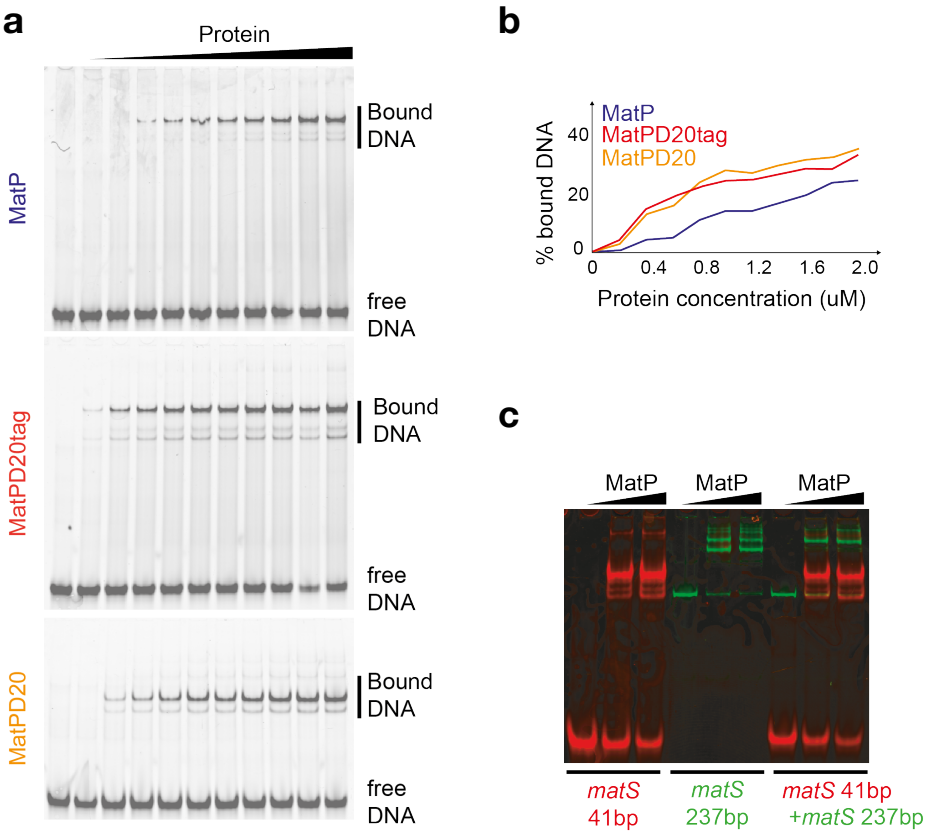

Figure S7: MatP interaction with DNA analysed by EMSA

a EMSA experiment showing the interaction between an increasing concentration of protein (0.2, 0.4, 0.6, 0.8, 1, 1.2, 1.4, 1.6, 1.8, and 2µM) and a 41bp DNA fragment containing *matS*. Top: purified MatP protein. Middle: purified tagged MatPΔ20 protein. Bottom: purified untagged MatPΔ20 protein. **b** Percentage of bound DNA was estimated (ImageJ) and plotted as a function of the protein concentration. **c** EMSA experiment showing the interaction between MatP (0, 3 and 6 µM) and a 41bp, Cy3-labeled DNA molecule containing *matS* or a 237bp, Cy5-labeled DNA molecule containing *matS*. Note that a DNA-protein complex made of two DNA molecules of different length bridged together by MatP would appear yellow on this gel.

a

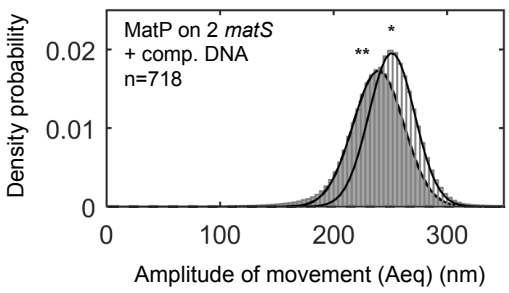

b

DNA construct	Unlooped lifetime (τ_{fast}, τ_{slow})(s)	Unlooped population	Number of events	Looped lifetime (τ_{fast}, τ_{slow})(s)	Looped population	Number of events
1 *matS*	16.5 ±7.0 147.9±42.9	0.44 0.56	719	10.0 ±1.2 72.0±22.5	0.42 0.58	488
2 *matS*	15.3 ±0.6 104.2±5.6	0.53 0.47	1,420	10.3 ±0.4 160.7±31.1	0.77 0.23	1,198

c

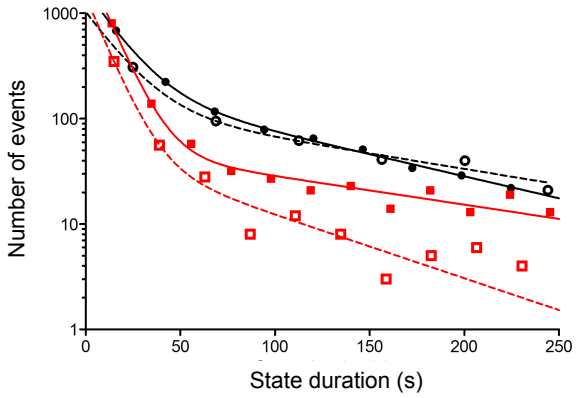

Figure S8: TPM with competitor DNA and kinetics analysis

a Probability distributions of Aeq, before protein injection (light grey histogram), or during the 5min following MatP injection (dark grey histogram). The DNA contained 2 *matS*, 2.5μM of competitor DNA (dsDNA, 40bp, non-specific) was added in the reaction, and the number of tracks is 718. *, population centred on (mean +/- SD) : 251 +/-20nm; **, population centred on (mean +/- SD): 238 +/- 24nm. **b** Table of the Gaussian fit results of TPM time traces. **c** Histogram of the durations of unlooped (Black) and looped (Red) for DNA containing one matS (hollow symbols) or 2 matS (full symbols) in presence of MatP.

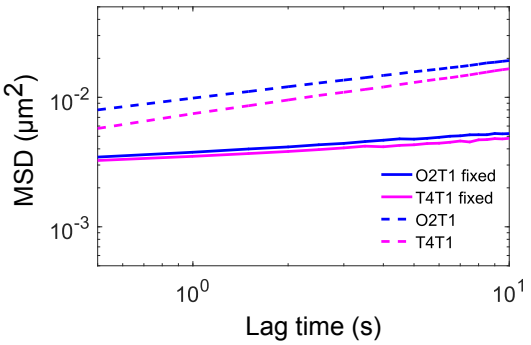

Figure S9: Mobility of foci in fixed cells

To assess the limitation of our detection system, a control was performed with fixed cells. Ori2 (blue curves) and Ter4 (pink curves) foci were followed as usual, and their MSD was calculated. The dotted lines show the medians of MSDs of foci for the non fixed cells used on the same day.